

Rotational dynamics of the asymmetric-top H₂O molecule induced by an intense laser field

Isamu Kikuchi,¹ Shinichi Fukahori ^{1,2} and Hirokazu Hasegawa ^{1,2,*}

¹*Department of Integrated Sciences, Graduate School of Arts and Sciences, The University of Tokyo, Komaba, Meguro-ku, Tokyo 153-8902, Japan*

²*Komaba Institute for Science, The University of Tokyo, Komaba, Meguro-ku, Tokyo 153-8902, Japan*



(Received 12 May 2023; accepted 23 June 2023; published 6 July 2023)

The rotational dynamics of the asymmetric-top H₂O molecule induced by an intense nonresonant laser pulse is investigated by a time-resolved pump-probe technique. The periodic rotational revival structure is not identified differently from the rotational dynamics of linear, symmetric, and near-symmetric top molecules. The rotational excitation processes are revealed based on the Fourier-transform spectrum of the H₂O⁺ yield observed as a function of the delay between the pump and probe pulses. In addition, by comparing with calculations, it is discussed whether one of two possibilities of the polarizability of H₂O reported previously is plausible.

DOI: [10.1103/PhysRevA.108.013101](https://doi.org/10.1103/PhysRevA.108.013101)

I. INTRODUCTION

An ultrashort intense nonresonant laser field imparts torque impulsively to a molecule via an anisotropic polarizability interaction. The induced field-free rotational dynamics has been widely investigated since the experimental observation [1,2] and theoretical works [3,4]. Recent developments and applications of the field-free rotational dynamics have been reviewed [5–8]. The rotational motion of weakly bound clusters has recently studied for Ar dimers [9], noble-gas dimers [10], CS₂ dimers [11], C₂H₂-He_{*n*} clusters [12], and C₂H₄ dimers and trimers [13,14], as well as the rotational motion of rigid molecules.

Studies on the field-free rotational dynamics for asymmetric-top molecules, which were reported much less than those for linear molecules, revealed the revival structure for iodobenzene (C₆H₅I) [15,16], pentafluoriodobenzene (C₆F₅I) [16], SO₂ [17,18], and ethylene (C₂H₄) [19,20], and the enhancement of the alignment degree by using a double pulse pair for C₆H₅I [21]. In addition to the one-dimensional alignment, the field-free three-dimensional alignment (FF3DA) for SO₂ [22], 3,5-difluoriodobenzene (C₆H₃F₂I) [23–25], and C₂H₄ [26] have been achieved. In the FF3DA, the rotational motion of SO₂ in a plane is induced by an optical centrifuge [27]. Moreover, the field-free one-dimensional orientation for C₆H₅I [28] and three-dimensional orientation (FF3DO) for 3,4-dibromothiophene (C₄H₂Br₂S) [29] and SO₂ [30] have been attained. In addition, the angular dependence of the ionization and dissociation probabilities for C₂H₄ has been studied using the field-free rotational dynamics [31].

The geometrical structure and the rotational energy structure are important factors for the rotational dynamics. Ray's asymmetry parameter, defined as $\kappa = \frac{2B-A-C}{A-C}$, is a measure to characterize the degree of asymmetry and a rotational energy level structure, where *A*, *B*, and *C* are rotational constants

in descending order (*A* > *B* > *C*). The asymmetry parameter ranges from $\kappa = -1$ for a prolate top to 1 for an oblate top. Molecules with $\kappa = 0$ are highly asymmetric from a structural perspective. Previous studies on the field-free rotational dynamics were limited to relatively low asymmetric molecules ranging from $|\kappa| = 0.99$ (3,4-dibromothiophene) to 0.74 (iodopentafluorobenzene).

In this paper, we investigate the field-free rotational dynamics and excitation processes of H₂O molecules with a high asymmetry of $\kappa = -0.44$. The rotational dynamics of H₂O is induced by an intense femtosecond pump pulse and H₂O⁺ ions are generated by another intense femtosecond probe pulse. From the measurement of the dependence of the H₂O⁺ yield on the delay between the pump and probe pulses, the rotational dynamics induced by the pump pulse is probed. In numerical calculations of the rotational dynamics, the components of a polarizability tensor in a molecular-fixed frame are required. However, two data sets of the polarizability of H₂O molecule were experimentally obtained [32] and are under discussion [33]. We also discuss which data sets are plausible.

II. EXPERIMENT

The experimental setup is almost the same as in the previous experiment [34]. Briefly, a light pulse from a Ti:sapphire femtosecond laser system (784 nm, 5 mJ/pulse, 130 fs, 10 Hz) was split into a pair of linearly polarized pump and probe pulses with a Michelson interferometer. They were focused onto a sample gas of the mixture of H₂O vapor at 50 °C, N₂ (20 kPa) as the reference gas, and Ne (180 kPa) as the buffer gas using a planoconvex lens with a focal length of 400 mm. The sample gas was introduced into a vacuum chamber with a time-of-flight (TOF) mass spectrometer as a supersonic molecular beam. The polarization direction of the pump and probe pulses was set to be parallel to the TOF axis. The yields of N₂⁺ and H₂O⁺ ionized by the probe pulse following the irradiation of the pump pulse, which creates rotational

*chs36@mail.ecc.u-tokyo.ac.jp

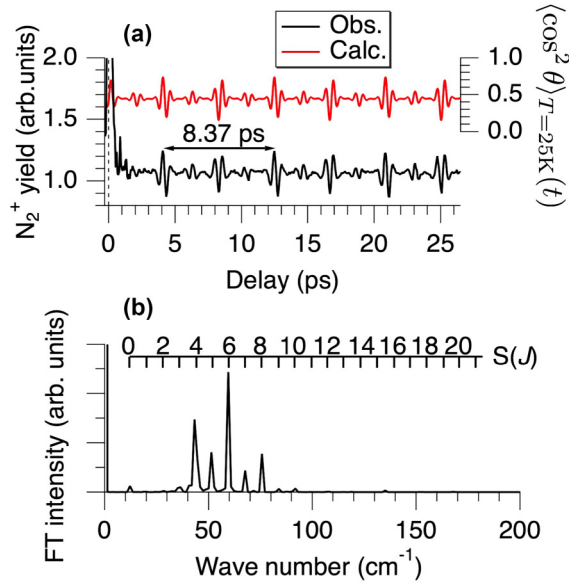


FIG. 1. (a) The dependence of the N_2^+ yield on the pump-probe delay (black curves) and the $\langle \cos^2 \theta \rangle_{T=25\text{K}}$ calculated using a rotational temperature of 25 K, a pulse duration of 130 fs, and an intensity of 35 TW/cm^2 (red curve). (b) The Fourier transform spectrum of the observed signal.

wave packets of N_2 and H_2O , were simultaneously measured as a function of the delay between the pump and probe pulses with a time interval of 67 fs. The delay dependence of the ion yields was measured 19 times and averaged. The intensities of the pump and probe pulses were experimentally estimated to be 100 and 200 TW/cm^2 , respectively, from the measured pulse width, beam diameter, and pulse energy. In order to reduce the effect of the energy fluctuation of the probe pulse (about 10%) on the ion yield, the pump pulse was chopped once every two laser shots and the ion yield measured with the pump pulse was divided by that without the pump pulse. In addition, the relative energy of the laser pulse was monitored with a photodiode shot by shot.

III. RESULTS AND DISCUSSION

Figure 1(a) shows the dependence of the N_2^+ yield on the delay between the pump and probe pulses. As reported previously [35], the revival structure is observed at the delay of multiples of a quarter, half, and full revival time. The observed revival time of $8.37(3)\text{ ps}$ corresponds to the rotational period of $T = 1/(2cB_0) = 8.38\text{ ps}$ in the vibrational ground state, where c is the speed of light in a vacuum, and the rotational constant in the vibrational ground state is $B_0 = 1.989574\text{ cm}^{-1}$ [36]. The horizontal axis of the observed signal is positively offset by 60 fs, which is less than one delay step, so that the observed signal coincides with the calculated $\langle \cos^2 \theta \rangle_{T=25\text{K}}(t)$ shown in Fig. 1(a), where $\langle \cos^2 \theta \rangle_{T=25\text{K}}(t)$ represents the thermally averaged expectation value of $\cos^2 \theta$ at the rotational temperature T [37] and θ is the angle between the N-N molecular axis and the polarization direction of the pump pulse.

The time variation of $\langle \cos^2 \theta \rangle_{T=25\text{K}}(t)$ reproduces the observed delay dependence of the N_2^+ yield when the pump

intensity of 35 TW/cm^2 , the rotational temperature of $T = 25\text{ K}$, and the pulse duration of 130 fs are adopted. The experimentally determined pump intensity of 100 TW/cm^2 is overestimated about three times. The overestimation may be the spatial inhomogeneous distribution of the pump intensity.

Figure 1(b) shows the Fourier-transform (FT) spectrum of the delay dependence of the observed N_2^+ yield. The peaks appearing in the FT spectrum are assigned as an S branch corresponding to the sequence of the rotational energy differences with $\Delta J = 2$, where J is a quantum number of a rotational angular momentum. These assignments mean that the rotational wave packet is created by the pump pulse through the impulsive rotational Raman processes. In addition, the peak positions in the FT spectrum match the rotational energy differences of the S branch, ensuring that the time interval of the horizontal axis in the delay signal is accurate. Since the rotational temperature and laser intensity are lower than those of the previous reports [38,39], the observed maximum J in the S branch is limited up to $J = 10$.

Figure 2(a) shows the observed H_2O^+ yield as a function of the delay, in which the offset of 60 fs is commonly adopted in the horizontal axis as in the N_2^+ signal. The delay dependence of the H_2O^+ yield differs from that of the N_2^+ yield in showing fast oscillation with a period of hundreds of femtoseconds and no clear revival structure. In addition, the J -type, A -type, and C -type revivals in the terminology of the rotational coherent spectroscopy [40] for near-prolate asymmetric tops [16–18,21,23,27] are not also identified due to the relatively higher structural asymmetry of H_2O . Although the periodicity in the delay-dependent H_2O^+ yield is unclear, many peaks appear in its FT spectrum as shown in Fig. 2(b). Each peak is assigned to the rotational energy differences, $J_{K_a, K_c} = 2_{1,1} - 1_{1,1}, 2_{0,2} - 0_{0,0}, 3_{1,2} - 2_{1,2}, 2_{2,1} - 1_{0,1}, 3_{0,3} - 1_{0,1}, 3_{1,2} - 1_{1,0}, 2_{2,0} - 0_{0,0}$, and $3_{2,1} - 1_{0,1}$ as shown in Fig. 2(c), where J_{K_a, K_c} represents the label of a rotational eigenstate and J , K_a , and K_c are the quantum numbers of a rotational angular momentum, the projection of the rotational angular momentum onto the molecular-fixed a axis in the prolate symmetric-top limit, and the c axis in the oblate-top limit, respectively.

As discussed above, the rotational temperature in the sample gas is estimated to be 25 K based on the N_2 result. Considering this temperature and nuclear spin statistics, the initial population of $0_{0,0}, 1_{0,1}, 1_{1,1}, 1_{1,0}, 2_{0,2}$, and $2_{1,2}$ is estimated to be 17%, 53%, 6%, 18%, 2%, and 4%, respectively. From the selection rules of the anisotropic polarizability interaction induced by a linearly polarized laser field [5–8], $\Delta J = 0, \pm 1, \pm 2$ for $M \neq 0$, $\Delta J = 0, \pm 2$ for $M = 0$, $ee(o) \leftrightarrow ee(o)$, and $eo(oe) \leftrightarrow eo(oe)$ for asymmetric-top molecules, it is found that the wave packets created by the pump pulse are composed of the rotational eigenstates, $\{0_{0,0}(0), 2_{0,2}(0), 2_{2,0}(0)\}, \{1_{0,1}(0), 3_{0,3}(0), 3_{2,1}(0)\}, \{1_{0,1}(\pm 1), 2_{2,1}(\pm 1), 3_{0,3}(\pm 1), 3_{2,1}(\pm 1)\}, \{1_{1,0}(0), 3_{1,2}(0)\}, \{1_{1,0}(\pm 1), 2_{1,2}(\pm 1), 3_{1,2}(\pm 1)\}$, and $\{1_{1,1}(\pm 1), 2_{1,1}(\pm 1)\}$, where M is a quantum number of the projection of the angular momentum J onto the pump laser polarization direction and the values in parentheses represent the value of M , i.e., $J_{K_a, K_c}(M)$. The labels of ee , eo , oe , and oo mean the even or odd numbers

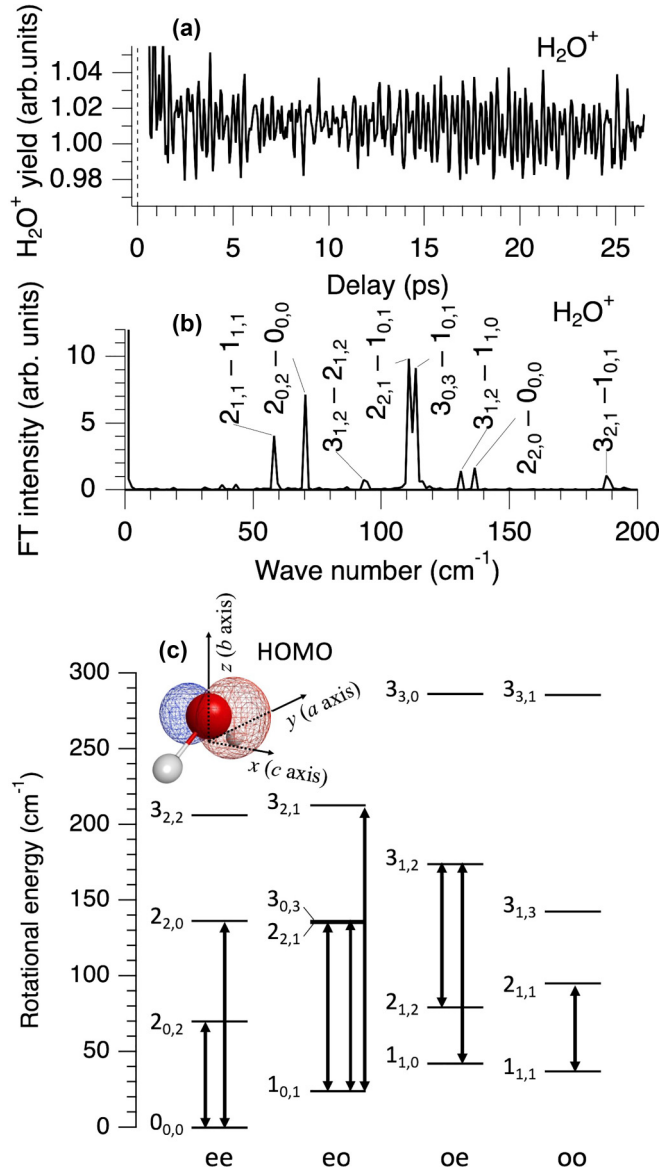


FIG. 2. (a) The dependence of the H₂O⁺ yield on the pump-probe delay. (b) The Fourier-transform spectrum of (a). (c) The calculated rotational energy levels with the assignment of peaks in the FT spectrum are shown as double-headed arrows. The shapes of the highest occupied molecular orbital (HOMO) and molecular-fixed axes are also shown in the inset. The labels of ee, eo, oe, and oo in the bottom represent the even or odd numbers for K_a, K_c.

for K_a and K_c. For example, the rotational level labeled by eo has even K_a and odd K_c. The FT peaks corresponding to the energy difference between 1_{1,1} and 3_{1,3}, which should appear at 105 cm⁻¹, are not observed in the FT spectrum.

In order to understand the excitation processes in detail, the time-dependent Schrödinger equation (TDSE) is numerically solved. In the calculation, the time-dependent rotational state is expanded by the field-free rotational eigenfunctions $\phi_{J_{K_a, K_c}}$ as follows,

$$\Psi_{J_{K_a^0, K_c^0}}^{J_{K_a^0, K_c^0}}(t) = \sum_J \sum_{K_a} \sum_{K_c} c_{J_{K_a, K_c}}^{J_{K_a^0, K_c^0}}(t) e^{-i \frac{E_{J_{K_a, K_c}}}{\hbar} t} \phi_{J_{K_a, K_c}}, \quad (1)$$

where $J_{K_a^0, K_c^0}^0$ is an initial rotational eigenstate, $E_{J_{K_a, K_c}}$ is a rotational eigenenergy of the rotational eigenstate J_{K_a, K_c} , and $c_{J_{K_a, K_c}}^{J_{K_a^0, K_c^0}}(t)$ is a time-dependent expansion coefficient. The following TDSE,

$$i\hbar \frac{d}{dt} \Psi_{J_{K_a^0, K_c^0}}^{J_{K_a^0, K_c^0}}(t) = \{\hat{H}_0 + \hat{V}(t)\} \Psi_{J_{K_a^0, K_c^0}}^{J_{K_a^0, K_c^0}}(t), \quad (2)$$

$$\begin{aligned} \hat{H}_0 = & \frac{1}{2}(B+C)\hat{J}^2 + \left\{ A - \frac{1}{2}(B+C) \right\} \hat{J}_a^2 \\ & + \frac{1}{4}(B-C)(\hat{J}^{+2} + \hat{J}^{-2}), \end{aligned} \quad (3)$$

$$\begin{aligned} \hat{V} = & \frac{1}{4}E^2(t) \left[\sqrt{\frac{1}{3}}\alpha_0^0 - \sqrt{\frac{2}{3}}\{D_{00}^{2*}(\chi, \theta, \phi)\alpha_0^2 \right. \\ & \left. + [D_{02}^{2*}(\chi, \theta, \phi) + D_{0-2}^{2*}(\chi, \theta, \phi)]\alpha_2^2 \right], \end{aligned} \quad (4)$$

is solved numerically using an adaptive step-size control Runge-Kutta method [41], where \hat{H}_0 is a field-free rigid-rotor Hamiltonian, \hat{V} is an anisotropic polarizability interaction of H₂O with a linearly polarized intense laser field [5–8] and with the nonresonant condition, A , B , and C are the rotational constants about molecular-fixed a , b , and c axes in the vibronic ground state, respectively, \hat{J} is a rotational angular momentum, \hat{J}_a is its projection onto the a axis, \hat{J}^{\pm} are raising and lowering operators of the rotational angular momentum referred to the molecular-fixed coordinate, $E(t)$ is an envelope function of an electric field for the pump laser pulse assumed to be a Gaussian function, α_q^k represents the q th spherical tensor component of a polarizability tensor of rank k , D_{pq}^J stands for the pq component of the Wigner's D matrix of rank J , and χ, θ, ϕ are the Euler angles relating the space-fixed XYZ axes to the molecular-fixed xyz axes. The molecular-fixed axes, defined as increasing order of the moment of inertia, a , b , and c axes, are assigned to the molecular-fixed, y , z , and x axes, respectively, as shown in the inset in Fig. 2(c). The rotational eigenenergies $E_{J_{K_a, K_c}}$ are obtained by diagonalization [41] of the field-free rotational Hamiltonian matrix \mathbf{H}_0 using Wang's basis function [42] and the rotational constants of $A = 27.8761$ cm⁻¹, $B = 14.5074$ cm⁻¹, and $C = 9.2877$ cm⁻¹ [43] and are shown in Fig. 2(c). The interaction with the pump laser pulse \hat{V} does not change the quantum number of the projection of the rotational angular momentum onto the polarization axis M because of the axial symmetry. Therefore, M is omitted in Eq. (1). The values of the polarizability tensor of H₂O molecule used in our calculation are discussed later.

Figures 3(a)–3(g) show the time dependence of the population, $|C_{J_{K_a, K_c}}^{J_{K_a^0, K_c^0}}(t)|^2$ for the initial states, $J_{K_a^0, K_c^0}^0(M) = 0_{0,0}(0)$, $1_{0,1}(0)$, $1_{0,1}(\pm 1)$, $1_{1,0}(0)$, $1_{1,0}(\pm 1)$, $1_{1,1}(0)$, and $1_{1,1}(\pm 1)$, respectively. The initial state $0_{0,0}(0)$ is excited to $2_{0,2}(0)$ and $2_{2,0}(0)$ simultaneously by the rotational Raman process as shown in Fig. 3(a). The excitation from the $0_{0,0}(0)$ state to the $1_{K_a, K_c}(0)$ state cannot occur because $\Delta J = \pm 1$ is forbidden for the $M = 0$ state. Therefore, the created rotational wave

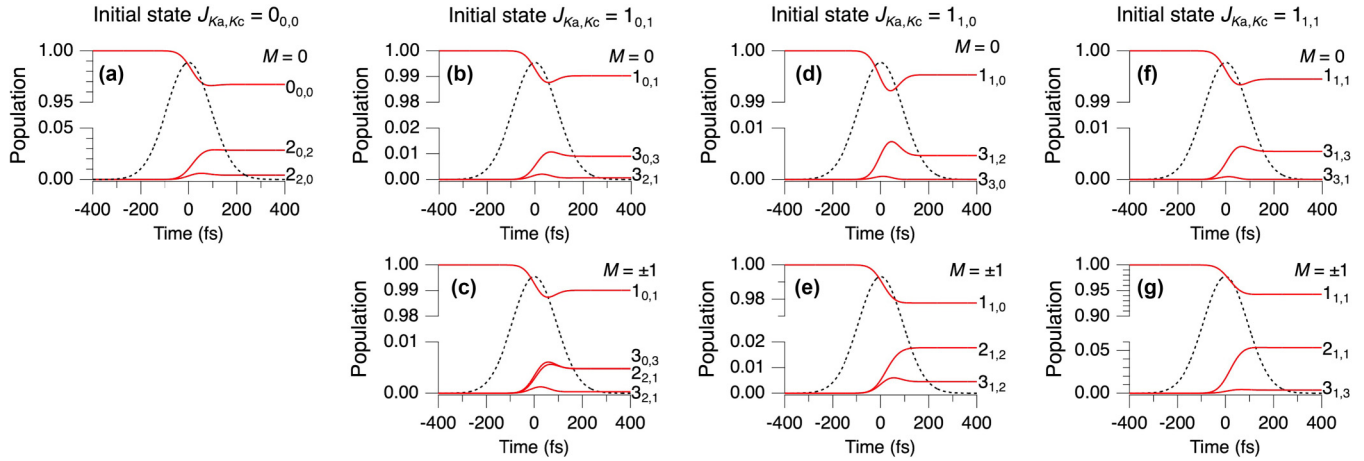


FIG. 3. The time dependence of the rotational population when the initial states are (a) $0_{0,0}$, (b) $1_{0,1}(0)$, (c) $1_{0,1}(\pm 1)$, (d) $1_{1,0}(0)$, (e) $1_{1,0}(\pm 1)$, (f) $1_{1,1}(0)$, and (g) $1_{1,1}(\pm 1)$. The dotted curves represent the envelope function of the laser intensity of 35 TW/cm^2 with the pulse width of 130 fs.

packet is composed of $0_{0,0}$, $2_{0,2}$, and $2_{2,0}$ states. The peaks in the FT spectrum appear at energy differences $2_{0,2} - 0_{0,0}$ (70 cm^{-1}) and $2_{2,0} - 0_{0,0}$ (136 cm^{-1}) as shown in Fig. 2(b). On the other hand, the peak corresponding to the energy difference between $2_{2,0}$ and $2_{0,2}$ (66 cm^{-1}) does not appear in the FT spectrum because the population of both $2_{0,2}$ and $2_{2,0}$ is small. The excitation processes are expressed as $[0_{0,0}(0) \rightarrow 2_{0,2}(0) \text{ and } 2_{2,0}(0)]$.

When the initial state is $1_{0,1}(0)$ as shown in Fig. 3(b), the only $3_{0,3}$ state is excited after the interaction though both $3_{0,3}$ and $3_{2,1}$ states are populated during the interaction. It is the most probable that the excitation from the initial $1_{0,1}$ to $3_{2,1}$ is not effectively induced by the rotational Raman process because the energy difference between these states, 188 cm^{-1} , is much larger than the bandwidth of the pump pulse of 110 cm^{-1} estimated from the pulse width of 130 fs. On the other hand, the excitation to $3_{0,3}$ is more probable than that to $3_{2,1}$ because the energy difference between $1_{0,1}$ and $3_{0,3}$ is 113 cm^{-1} . The rotational energy differences of 113 and 188 cm^{-1} are recognized in the FT spectrum in Fig. 2(b). The weak peak at 188 cm^{-1} in the FT spectrum is consistent with the lower excitation to the $3_{2,1}$ state. When the initial state is $1_{0,1}(M = \pm 1)$, $2_{2,1}$ and $3_{0,3}$ states are excited simultaneously as shown in Fig. 3(c). The transition from $1_{0,1}$ to $2_{2,1}$ is allowed due to $M \neq 0$. The corresponding FT peak of 111 cm^{-1} is also identified in Fig. 2(b). The excitation processes are expressed as $[1_{0,1}(0) \rightarrow 3_{0,3}(0) \text{ and } 3_{2,1}(0)]$, $[1_{0,1}(\pm 1) \rightarrow 2_{2,1}(\pm 1), 3_{0,3}(\pm 1) \text{ and } 3_{2,1}(\pm 1)]$.

Figures 3(d) and 3(e) show the time dependence of the population when the initial states are $J_{Ka,Kc}^0(M) = 1_{1,0}(0)$ and $1_{1,0}(\pm 1)$, respectively. It is found that the initial state $J_{Ka,Kc}^0(M) = 1_{1,0}(0)$ is excited to only the $3_{1,2}$ state. Therefore, the created rotational wave packet is composed of $1_{1,0}$ and $3_{1,2}$ states. On the other hand, the initial state $1_{1,0}(\pm 1)$ is excited to $2_{1,2}$ and $3_{1,2}$ simultaneously. As a result, the created rotational wave packet is composed of eigenstates, $\{1_{1,0}, 2_{1,2}, 3_{1,2}\}$. The excitation from $1_{1,0}(0)$ to $2_{1,2}$ does not appear because the $\Delta J = 1$ transition for a $M = 0$ state is forbidden. The energy differences of $3_{1,2} - 2_{1,2}$ and $3_{1,2} - 1_{1,0}$ are recognized as the peaks at 94 and 131 cm^{-1} in

the FT spectrum, respectively. Similarly, the energy difference between $2_{1,2}$ and $1_{1,0}$ is expected to appear at around 37 cm^{-1} in the FT spectrum. However, this signal is absent. This peak may be assigned to a weak signal appearing at about 38 cm^{-1} . From Figs. 3(d) and 3(e), we found that the rotational population of $1_{1,0}$ state is transferred through the pathways, $[1_{1,0}(0) \rightarrow 3_{1,2}(0)]$ and $[1_{1,0}(\pm 1) \rightarrow 2_{1,2}(\pm 1) \text{ and } 3_{1,2}(\pm 1)]$.

Similarly, the excitation pathways, $[1_{1,1}(0) \rightarrow 3_{1,3}(0)]$ and $[1_{1,1}(\pm 1) \rightarrow 2_{1,1}(\pm 1) \text{ and } 3_{1,3}(\pm 1)]$, are identified as shown in Figs. 3(f) and 3(g), respectively.

All peaks in the FT spectrum are assigned to the energy differences between these rotational eigenstates. However, the peak of the energy difference between $1_{1,1}$ and $3_{1,3}$, 105 cm^{-1} , is not observed in the FT spectrum. It may be ascribed to the low population, $|c_{3_{1,3}}^{1_{1,1}}(t = \infty)|^2 < 0.005$ for $M = 0$ and ± 1 or inappropriate probe manner in which the probe pulse ionizes the electron in the highest occupied molecular orbital (HOMO). This point will be discussed in a forthcoming paper.

The expectation value of $\cos^2 \theta_{Zc}$ is calculated using the rotational wave packet $\Psi_{K_a^0, K_c^0}^0(t)$ in order to compare the delay dependence of the observed H_2O^+ yield, where θ_{Zc} is the angle between the space-fixed Z axis parallel to the pump polarization direction and the molecular-fixed $x(c)$ axis. The thermally averaged expectation value of $\cos^2 \theta_{Zc}$,

$$\langle \cos^2 \theta_{Zc} \rangle_{T=25 \text{ K}}(t) = \sum_{J^0, K_a^0, K_c^0} w_{K_a^0, K_c^0}^J g_{K_a^0, K_c^0} \langle \Psi_{K_a^0, K_c^0}^0(t) | \cos^2 \theta_{Zc} | \Psi_{K_a^0, K_c^0}^0(t) \rangle, \quad (5)$$

is calculated, where $w_{K_a^0, K_c^0}^J$ is a Boltzmann factor for the initial rotational state of $\phi_{K_a^0, K_c^0}^J$ and $g_{K_a^0, K_c^0}$ is a nuclear spin statistics weight, $g_{K_a^0, K_c^0} = 3$ for eo and oe states (ortho- H_2O) and $g_{K_a^0, K_c^0} = 1$ for ee and oo states (para- H_2O). The laser intensity, pulse duration, and rotational temperature used in the calculation are the same values as those in the N_2 calculation.

The values of three Cartesian polarizability components α_{aa} , α_{bb} , and α_{cc} in the molecular-fixed frame are required to calculate the TDSE numerically, where α_{ii} ($i = a, b, c$)

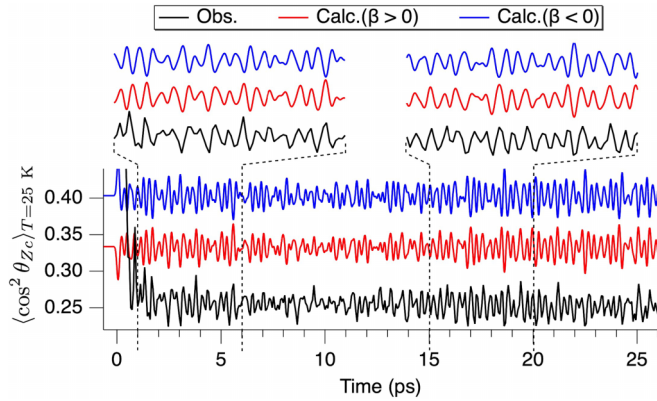


FIG. 4. The observed H_2O^+ yield as a function of the pump-probe delay (black curve) and the calculated $\langle \cos^2 \theta_{Zc} \rangle_{T=25 \text{ K}}(t)$ for $\beta > 0$ (red curve) and $\beta < 0$ (blue curve).

represents the polarizability component in the molecular-fixed coordinate, which is related to the spherical tensor components, $\alpha_0^0 = -\sqrt{\frac{1}{3}}(\alpha_{aa} + \alpha_{bb} + \alpha_{cc})$, $\alpha_0^2 = \sqrt{\frac{1}{6}}(2\alpha_{aa} - \alpha_{bb} - \alpha_{cc})$, and $\alpha_{\pm 2}^2 = \frac{1}{2}(\alpha_{bb} - \alpha_{cc})$ for H_2O [7]. The polarizability tensor components determined experimentally from a Rayleigh depolarization ratio, a rotational Raman spectrum, and a refractive index of water vapor were widely accepted [32]. However, the polarizability tensor components could not be determined uniquely in their experiment [32], but there were two data sets of the polarizability because the only square of β , $\beta^2 = \frac{3}{2}\{(\alpha_0^2)^2 + \frac{1}{2}(\alpha_2^2 + \alpha_{-2}^2)^2\}$, was determined from the experiment. Therefore, two data sets of the polarizabilities measured at a wavelength of 514.5 nm, $(\alpha_{aa}, \alpha_{bb}, \alpha_{cc}) = (1.5284, 1.4679, 1.4146)$ for $\beta > 0$ and $(\alpha_{aa}, \alpha_{bb}, \alpha_{cc}) = (1.4122, 1.4727, 1.5260)$ for $\beta < 0$, in units of \AA^3 , are available and adopted to solve the TDSE in our calculation. It should be noted that the polarizability of liquid water has been actively investigated and discussed [33].

Figure 4 shows the observed H_2O^+ yield as a function of the pump-probe delay and the calculated $\langle \cos^2 \theta_{Zc} \rangle_{T=25 \text{ K}}(t)$ for $\beta > 0$ and $\beta < 0$. It is found that the calculated signals for $\beta > 0$ and $\beta < 0$ are out of phase with each other by π . This result is explained by the sign of the spherical

polarizability tensor components (α_0^2 and $\alpha_{\pm 2}^2$), included in the interaction term of Eq. (4). The absolute values of α_0^2 and $\alpha_{\pm 2}^2$ for $\beta < 0$ and $\beta > 0$ are the same but their signs are opposite. In other words, $\alpha_0^2(\beta > 0) = -\alpha_0^2(\beta < 0)$ and $\alpha_{\pm 2}^2(\beta > 0) = -\alpha_{\pm 2}^2(\beta < 0)$ are satisfied. The observed signal agrees well with $\langle \cos^2 \theta_{Zc} \rangle_{T=25 \text{ K}}(t)$ calculated by using the polarizability data set with $\beta > 0$. Our time-resolved measurement of the rotational motion allows us to determine the sign of β securely. Similarly, the sign of the polarizability tensor responsible for the spin-orbit electronic Raman transition was also determined from a similar experiment [34].

The agreement between the observation and calculation is interpreted as an electron ejection from the HOMO by the tunneling ionization induced by the probe pulse. The shape of the HOMO shown in the inset of Fig. 2(c), which corresponds to the nonbonding $2p_x$ orbital of the O atom, spreads along the $x(c)$ axis perpendicular to the molecular plane. Therefore, the ionization probability is enhanced when the polarization direction of the ionization pulse is parallel to the molecular $x(c)$ axis. As a result, the delay dependence of the observed H_2O^+ yields agrees with the calculated $\langle \cos^2 \theta_{Zc} \rangle_{T=25 \text{ K}}(t)$. The ionization from the HOMO is consistent with the isolation of the H_2O^+ electronic ground \tilde{X}^2B_1 state from the other electronic states, where the vertical ionization potential of 12.6223 and 14.6398 eV needed to generate the \tilde{X}^2B_1 and \tilde{A}^2A_1 electronic states in H_2O^+ , respectively [44].

In summary, the rotational dynamics of H_2O was investigated by measuring the dependence of the H_2O^+ yield on the delay between the pump rotational excitation pulse and the probe ionization pulse. The fast and complicated rotational dynamics were observed. On the basis of the analysis of the FT spectrum, the excitation processes were identified. The agreement between the calculated $\langle \cos^2 \theta_{Zc} \rangle_{T=25 \text{ K}}(t)$ and the observed delay dependence of the H_2O^+ yield revealed that the electron is emitted from the HOMO to create H_2O^+ . In addition, the sign of the spherical polarizability tensor was determined with the aid of the time-resolved manner.

ACKNOWLEDGMENT

This work was supported by JSPS KAKENHI Grants No. JP21K18143, No. JP23H01918, and No. JP23K13705.

- [1] J. P. Heritage, T. K. Gustafson, and C. H. Lin, Observation of Coherent Transient Birefringence in CS_2 Vapor, *Phys. Rev. Lett.* **34**, 1299 (1975).
- [2] F. Rosca-Pruna and M. J. J. Vrakking, Experimental Observation of Revival Structures in Picosecond Laser-Induced Alignment of I_2 , *Phys. Rev. Lett.* **87**, 153902 (2001).
- [3] I. S. Averbukh and N. F. Perelman, Fractional revivals: Universality in the long-term evolution of quantum wave packets beyond the correspondence principle dynamics, *Phys. Lett. A* **139**, 449 (1989).
- [4] T. Seideman, Rotational excitation and molecular alignment in intense laser fields, *J. Chem. Phys.* **103**, 7887 (1995).
- [5] H. Stapelfeldt and T. Seideman, Colloquium: Aligning molecules with strong laser pulses, *Rev. Mod. Phys.* **75**, 543 (2003).
- [6] T. Seideman and E. Hamilton, Nonadiabatic alignment by intense pulses. Concepts, theory, and directions, *Adv. At. Mol. Opt. Phys.* **52**, 289 (2005).
- [7] Y. Ohshima and H. Hasegawa, Coherent rotational excitation by intense nonresonant laser fields, *Int. Rev. Phys. Chem.* **29**, 619 (2010).
- [8] C. P. Koch, M. Lemeshko, and D. Sugny, Quantum control of molecular rotation, *Rev. Mod. Phys.* **91**, 035005 (2019).
- [9] J. Wu, A. Vredenburg, B. Ulrich, L. Ph. H. Schmidt, M. Meckel, S. Voss, H. Sann, H. Kim, T. Jahnke, and R. Dörner, Nonadiabatic alignment of van der Waals-force-bound argon dimers by femtosecond laser pulses, *Phys. Rev. A* **83**, 061403(R) (2011).
- [10] A. von Veltheim, B. Borchers, G. Steinmeyer, and H. Rottke, Imaging the impulsive alignment of noble-gas dimers via Coulomb explosion, *Phys. Rev. A* **89**, 023432 (2014).

- [11] A. S. Chatterley, M. O. Bastrup, C. A. Schouder, and H. Stapelfeldt, Laser-induced alignment dynamics of gas phase CS₂ dimers, *Phys. Chem. Chem. Phys.* **22**, 3245 (2020).
- [12] G. Galinis, C. Cacho, R. T. Chapman, A. M. Ellis, M. Lewerenz, L. G. M. Luna, R. S. Minns, M. Mladenović, A. Rouzée, E. Springate, I. C. E. Turcu, M. J. Watkins, and K. von Haeften, Probing the Structure and Dynamics of Molecular Clusters Using Rotational Wave Packets, *Phys. Rev. Lett.* **113**, 043004 (2014).
- [13] Y. Ohshima, Y. Tobata, and K. Mizuse, Rotational wave-packet imaging spectroscopy of the ethylene dimer, *Chem. Phys. Lett.* **803**, 139850 (2022).
- [14] K. Mizuse, K. Takano, E. Kakizaki, Y. Tobata, and Y. Ohshima, Time-domain rotational Raman spectroscopy of the ethylene dimer and trimer by Coulomb explosion imaging of rotational wave packets, *J. Phys. Chem. A* **127**, 4848 (2023).
- [15] E. Péronne, M. D. Poulsen, C. Z. Bisgaard, H. Stapelfeldt, and T. Seideman, Nonadiabatic Alignment of Asymmetric Top Molecules: Field-Free Alignment of Iodobenzene, *Phys. Rev. Lett.* **91**, 043003 (2003).
- [16] M. D. Poulsen, E. Péronne, H. Stapelfeldt, C. Z. Bisgaard, S. S. Viftrup, E. Hamilton, and T. Seideman, Nonadiabatic alignment of asymmetric top molecules: Rotational revivals, *J. Chem. Phys.* **121**, 783 (2004).
- [17] R. Damari, S. Kallush, and S. Fleischer, Rotational Control of Asymmetric Molecules: Dipole- versus Polarizability-Driven Rotational Dynamics, *Phys. Rev. Lett.* **117**, 103001 (2016).
- [18] I. F. Tenney, M. Artamonov, T. Seideman, and P. H. Bucksbaum, Collisional decoherence and rotational quasirevivals in asymmetric-top molecules, *Phys. Rev. A* **93**, 013421 (2016).
- [19] J. G. Underwood, B. J. Sussman, and A. Stolow, Field-Free Three Dimensional Molecular Axis Alignment, *Phys. Rev. Lett.* **94**, 143002 (2005).
- [20] A. Rouzée, S. Guérin, V. Boudon, B. Lavorel, and O. Faucher, Field-free one-dimensional alignment of ethylene molecule, *Phys. Rev. A* **73**, 033418 (2006).
- [21] C. Z. Bisgaard, M. D. Poulsen, E. Péronne, S. S. Viftrup, and H. Stapelfeldt, Observation of Enhanced Field-Free Molecular Alignment by Two Laser Pulses, *Phys. Rev. Lett.* **92**, 173004 (2004).
- [22] K. F. Lee, D. M. Villeneuve, P. B. Corkum, A. Stolow, and J. G. Underwood, Field-Free Three-Dimensional Alignment of Polyatomic Molecules, *Phys. Rev. Lett.* **97**, 173001 (2006).
- [23] S. S. Viftrup, V. Kumarappan, S. Trippel, H. Stapelfeldt, E. Hamilton, and T. Seideman, Holding and Spinning Molecules in Space, *Phys. Rev. Lett.* **99**, 143602 (2007).
- [24] S. S. Viftrup, V. Kumarappan, L. Holmegaard, C. Z. Bisgaard, H. Stapelfeldt, M. Artamonov, E. Hamilton, and T. Seideman, Controlling the rotation of asymmetric top molecules by the combination of a long and a short laser pulse, *Phys. Rev. A* **79**, 023404 (2009).
- [25] X. Ren, V. Makhija, and V. Kumarappan, Multipulse Three-Dimensional Alignment of Asymmetric Top Molecules, *Phys. Rev. Lett.* **112**, 173602 (2014).
- [26] A. Rouzée, S. Guérin, O. Faucher, and B. Lavorel, Field-free molecular alignment of asymmetric top molecules using elliptically polarized laser pulses, *Phys. Rev. A* **77**, 043412 (2008).
- [27] A. Korobenko and V. Milner, Adiabatic Field-Free Alignment of Asymmetric Top Molecules with an Optical Centrifuge, *Phys. Rev. Lett.* **116**, 183001 (2016).
- [28] J. H. Mun, D. Takei, S. Minemoto, and H. Sakai, Laser-field-free orientation of state-selected asymmetric top molecules, *Phys. Rev. A* **89**, 051402(R) (2014).
- [29] D. Takei, J. H. Mun, S. Minemoto, and H. Sakai, Laser-field-free three-dimensional molecular orientation, *Phys. Rev. A* **94**, 013401 (2016).
- [30] K. Lin, I. Tutunnikov, J. Qiang, J. Ma, Q. Song, Q. Ji, W. Zhang, H. Li, F. Sun, X. Gong, H. Li, P. Lu, H. Zeng, Y. Prior, I. S. Averbukh, and J. Wu, All-optical field-free three-dimensional orientation of asymmetric-top molecules, *Nat. Commun.* **9**, 5134 (2018).
- [31] V. Makhija, X. Ren, D. Gockel, A.-T. Le, and V. Kumarappan, Orientation resolution through rotational coherence spectroscopy, [arXiv:1611.06476](https://arxiv.org/abs/1611.06476).
- [32] W. F. Murphy, The rayleigh depolarization ratio and rotational Raman spectrum of water vapor and the polarizability components for the water molecule, *J. Chem. Phys.* **67**, 5877 (1977).
- [33] P. Zalden, L. Song, X. Wu, H. Huang, F. Ahr, O. D. Mücke, J. Reichert, M. Thorwart, P. K. Mishra, R. Welsch, R. Santra, F. X. Kärtner, and C. Bressle, Molecular polarizability anisotropy of liquid water revealed by terahertz-induced transient orientation, *Nat. Commun.* **9**, 2142 (2018).
- [34] S. Fukahori, A. Iwasaki, K. Yamanouchi, and H. Hasegawa, Single and sequential double ionization of no radical in intense laser fields, *J. Chem. Phys.* **156**, 094307 (2022).
- [35] T. Kanai, S. Minemoto, and H. Sakai, Quantum interference during high-order harmonic generation from aligned molecules, *Nature (London)* **435**, 470 (2005).
- [36] J. Bendtsen, The rotational and rotation-vibrational Raman spectra of ¹⁴N₂, ¹⁴N ¹⁵N and ¹⁵N₂, *J. Raman Spectrosc.* **2**, 133 (1974).
- [37] M. Tsubouchi and T. Suzuki, Photoionization of homonuclear diatomic molecules aligned by an intense femtosecond laser pulse, *Phys. Rev. A* **72**, 022512 (2005).
- [38] P. W. Dooley, I. V. Litvinyuk, Kevin F. Lee, D. M. Rayner, M. Spanner, D. M. Villeneuve, and P. B. Corkum, Direct imaging of rotational wave-packet dynamics of diatomic molecules, *Phys. Rev. A* **68**, 023406 (2003).
- [39] K. Miyazaki, M. Kaku, G. Miyaji, A. Abdurrouf, and F. H. M. Faisal, Field-Free Alignment of Molecules Observed with High-Order Harmonic Generation, *Phys. Rev. Lett.* **95**, 243903 (2005).
- [40] P. M. Felker, Rotational coherence spectroscopy: Studies of the geometries of large gas-phase species by picosecond time-domain methods, *J. Phys. Chem.* **96**, 7844 (1992).
- [41] W. H. Press, S. A. Teukolsky, W. T. Vetterling, and B. P. Flannery, *Numerical Recipes in C* (Cambridge University Press, Cambridge, UK, 1992).
- [42] S. C. Wang, On the asymmetrical top in quantum mechanics, *Phys. Rev.* **34**, 243 (1929).
- [43] R. T. Hall and J. M. Dowling, Pure rotational spectrum of water vapor, *J. Chem. Phys.* **47**, 2454 (1967).
- [44] J. E. Reutt, L. S. Wang, Y. T. Lee, and D. A. Shirley, Molecular beam photoelectron spectroscopy and femtosecond intramolecular dynamics of H₂O⁺ and D₂O⁺, *J. Chem. Phys.* **85**, 6928 (1986).